

Final Report Biomechanics

Cruz Gómez Lucero del Rocío, Bernadet Pierre

March 2025

Contents

1	Background	3
2	Problem statement and focus topic	3
2.1	Design of the microneedle patch	3
2.1.1	Material Selection	3
2.1.2	Microneedle lenght	4
2.1.3	Base Diameter	4
2.1.4	Tip Diameter	4
2.1.5	Tip Angle	4
2.2	Parameters of skin layers	4
2.2.1	Stratum Corneum	4
2.2.2	Epidermis	5
2.2.3	Dermis	5
2.3	Design 3D of the microneedle patch in SOLIDWORKS	6
2.4	Mathematical problem statement for analytical and numerical solving methods	6
2.4.1	Simplest model	6
2.4.2	Complex model	7
2.5	COMSOL problem statement	8
2.5.1	Geometry and Layers	8
2.5.2	Boundary Conditions	8
2.5.3	Domains and Parameters	9
2.5.4	Simulation Time	9
2.6	Focus topic	9
3	Methods	9
3.1	Analytical method	9
3.2	Numerical simplest model	10
3.3	Numerical complex model	11
3.4	COMSOL modelisation	12
4	Results	12
4.1	Analytical and numerical method provide same results	12
4.2	Results of the Simplest model	13
4.2.1	Analysis of the effect of diffusion coefficient	13
4.2.2	Analysis of the effect of initial concentration	14
4.2.3	Analysis of the effect of microneedle length	15
4.2.4	Analysis of the drug delivery profiles	15
4.3	Results of the Complex model	16

4.3.1	Analysis of the effect of diffusion coefficient	18
4.3.2	Analysis of the effect of microneedle length	18
4.3.3	Analysis of the effect of initial concentration	19
4.4	Results on COMSOL	19
4.4.1	Microneedle lenght	19
4.4.2	Intlet velocity	21
5	Critique and summary	22
5.1	Critiques on the numerical model	22
6	Recommendations for future work	22
7	References	23

1 Background

Microneedle patches represent a promising technology in the field of transdermal drug delivery, offering a minimally invasive alternative to conventional hypodermic needles. These patches consist of an array of microscopic needles, typically fabricated from biocompatible materials such as polymers, silicon, or metals, which penetrate the outermost layers of the skin to deliver therapeutic agents directly into the systemic circulation or localized tissue. The mechanism of action involves the creation of microchannels through the skin layers, bypassing the stratum corneum, which is the primary barrier to drug permeation, thereby enhancing bioavailability and reducing systemic side effects.

The human skin is composed of multiple layers, with the epidermis serving as the outermost protective barrier. The epidermis includes several sublayers, namely the stratum corneum, stratum lucidum, stratum granulosum, stratum spinosum, and stratum basale. Among these, the stratum corneum is the thickest and most crucial for transdermal applications, with an average thickness of approximately 10-20 μm in most body areas (Barry, 2001). The stratum lucidum, present mainly in thick skin such as the palms and soles, measures around 20-30 μm , while the entire epidermal thickness ranges between 50-100 μm , depending on the anatomical site (Scheuplein & Blank, 1971).

For optimal drug delivery, microneedles must be designed to effectively bypass the stratum corneum without penetrating too deeply into the dermis, which contains nerve endings and blood vessels. Studies suggest that microneedles with lengths ranging from 150 to 900 μm are effective for achieving efficient drug transport while minimizing discomfort (Donnelly et al., 2012). The relationship between microneedle length and the stratum corneum thickness is critical; microneedles should ideally be at least 1.5 times the thickness of the stratum corneum to ensure successful transdermal delivery. For example, with a stratum corneum thickness of 20 μm , a microneedle length of approximately 30 μm would be necessary to achieve adequate penetration and drug diffusion (Prausnitz et al., 2004).

Mathematical models for transdermal drug delivery are essential for predicting drug diffusion kinetics and optimizing microneedle design. These models commonly utilize Fick's laws of diffusion to describe the passive transport of drug molecules across the skin barrier (Guy & Hadgraft, 2003). Additionally, multilayer diffusion models consider the varying permeability coefficients of different skin layers, accounting for the stratum corneum's high resistance and the faster transport through deeper layers (Langer & Peppas, 1983). Finite element modeling (FEM) and compartmental models have also been employed to simulate complex drug release profiles and skin interactions, offering insights into optimization strategies for microneedle patches (Kwon et al., 2017)

2 Problem statement and focus topic

2.1 Design of the microneedle patch

The design of the micro-needle patch described here incorporates several parameters, including material selection, microneedle length, base diameter, tip diameter and tip angle, each chosen to optimize its performance.

2.1.1 Material Selection

The microneedles are fabricated from titanium alloy Ti6Al4V, a material chosen for its exceptional mechanical strength, biocompatibility, and corrosion resistance (Geetha et al., 2009; Niinomi, 2008). Titanium alloys are widely used in medical implants due to their ability to withstand physiological conditions without degrading or causing adverse immune responses (Elias et al., 2008). Ti6Al4V, in particular, offers a high strength-to-weight ratio, ensuring that the microneedles are robust enough to penetrate the skin without breaking or bending (Leyens & Peters, 2003). Additionally, its biocompatibility minimizes the risk of inflammation or rejection, making it an ideal choice for prolonged or repeated use in biomedical applications (Brunette et al., 2001).

2.1.2 Microneedle length

Verbaan et al. (2007) tested a microneedle system with different lengths (300, 550, 700, and 900 μm). The study demonstrated that microneedles with a length of 300 μm could not penetrate human skin, while microneedles with a length above 550 μm successfully pierced skin. For this reason, the microneedle designed has a length of 750 micrometers. This length was selected to ensure penetration into the epidermis and upper dermis layers of the skin, while avoiding contact with nerve endings located deeper in the dermis.

2.1.3 Base Diameter

The base diameter is a factor that impact the structural integrity to prevent buckling or fracture during skin penetration. A wider base ensures stability when the patch is applied to the skin, enabling uniform distribution of force across the array of microneedles (Park et al., 2010). Kochhar et al. (2013) examined the impact of needle tip spacing, base diameter, and length on skin penetration. They found that a length of 827 μm and a base diameter of 200 μm resulted in a slower penetration rate compared to a base diameter of 300 μm and a length of 400 μm . Besides, in another study MN was analyzed with a length of 600 μm with a base diameter of 380 μm (Abdullah et al., 2024). Based on these studies and considering the tip diameter and tip angle, we defined the base diameter in 430 μm .

2.1.4 Tip Diameter

The microneedle tip diameter influences the contact area between the microneedle and the skin and, consequently, the insertion force. Small tips reduce insertion force, leading to a smaller skin deformation and minimizing tissue damage, thus a greater chance of penetration (Davis et al., 2004). In a study in 2014, the authors found that the smaller the needle tip diameter (5 μm), the smoother the penetration. On the other hand, with a larger tip diameter, the penetration of the system in human ex vivo skin was more abrupt. They also concluded that a tip diameter smaller or equal to 15 μm is fundamental for inserting microneedles into the desired depth of the skin in a well-controlled manner (Romgens et al.). For this reason, we considered a tip diameter 15 micrometers.

2.1.5 Tip Angle

Finally, the tip angle was the last parameter that we considered in our design. The angle must be optimized to ease the insertion of the needle through the skin. A sharper angle facilitates penetration into the skin with minimal resistance while maintaining the microneedle's structural integrity to prevent breakage (Oliveira et al., 2024). Bao et al. (2022) suggested that a tip angle of 30° can easily pierce the skin. Besides, in another article the authors also verified the tip angles (15–30°) using biodegradable microneedles (Sabri et al., 2020). For this reason, we chose 30° as the tip angle.

2.2 Parameters of skin layers

The skin is a complex organ composed of multiple layers, each with distinct structural and functional properties that contribute to the skin's overall role as a protective barrier, thermal regulator, and sensory organ. The three primary layers of interest are the stratum corneum, epidermis, and dermis. Below, we describe the thickness, density, thermal conductivity, specific heat, and diffusion coefficient of each layer.

2.2.1 Stratum Corneum

The stratum corneum is the outermost layer of the skin and forms the primary barrier against environmental factors such as pathogens, chemicals, and water loss. It is composed of dead, keratinized cells (corneocytes) embedded in a lipid matrix. This layer is relatively thin but highly effective in preventing transdermal water loss and protecting underlying tissues (Elias, 1983; Menon, 2002).

- Thickness: The stratum corneum has an average thickness of approximately 10 μm , though this can vary depending on the body region (Marquez-Lago et al., 2010)
- Density: The density of the stratum corneum is approximately 1.20 gm/cm^3 , reflecting its compact and keratinized structure (Anderson & Cassidy, 1973)
- Thermal Conductivity: The thermal conductivity of the stratum corneum is around $0.2 \text{ W/m}\cdot\text{K}$, which is relatively low due to its lipid-rich composition (Becker, 2012)
- Specific Heat: The specific heat capacity of the stratum corneum is approximately $3578 \text{ J/kg}\cdot\text{K}$, indicating its ability to store thermal energy (Fu et al., 2014)
- Diffusion Coefficient: The diffusion coefficient for small molecules through the stratum corneum is typically in the range of $1 \times 10^{-9} \text{ cm}^2/\text{s}$, reflecting its role as a barrier to transdermal transport (Nagayama & Kurihara, 2018).

2.2.2 Epidermis

Beneath the stratum corneum lies the epidermis, a living layer of skin that provides additional protection and houses melanocytes, which produce melanin for UV protection. The epidermis is avascular and relies on diffusion from the dermis for nutrient supply. It is thicker than the stratum corneum and plays a key role in immune response and wound healing (Proksch, Brandner, & Jensen, 2008).

- Thickness: The epidermis has an average thickness of 90 μm (Marquez-Lago et al., 2010)
- Density: The density of the epidermis is approximately 1200 kg/m^3 (Fu et al., 2014)
- Thermal Conductivity: The thermal conductivity of the epidermis is around $0.209 \text{ W/m}\cdot\text{K}$, which is higher than that of the stratum corneum due to its higher water content (Becker, 2012)
- Specific Heat: The specific heat capacity of the epidermis is approximately $3600 \text{ J/kg}\cdot\text{K}$ (Fu et al., 2014)
- Diffusion Coefficient: The diffusion coefficient for small molecules through the epidermis is typically in the range of $6.2 \times 10^{-5} \text{ mm}^2/\text{s}$ (Cornelissen et al., 2008).

2.2.3 Dermis

The dermis is the thickest layer of the skin and lies beneath the epidermis. It is composed of connective tissue, blood vessels, nerves, hair follicles, and sweat glands. The dermis provides structural support, elasticity, and strength to the skin. It also plays a critical role in thermoregulation through blood flow and sweat production (Sorrell & Caplan, 2004).

- Thickness: The dermis has an average thickness of approximately 1 mm, though this varies significantly depending on the body region (Marquez-Lago et al., 2010)
- Density: The density of the dermis is approximately 1200 kg/m^3 , reflecting its fibrous and collagen-rich structure (Li et al., 2012)
- Thermal Conductivity: The thermal conductivity of the dermis is around $0.293 \text{ W/m}\cdot\text{K}$, which is higher than that of the epidermis due to its vascularization and water content (Becker, 2012)
- Specific Heat: The specific heat capacity of the dermis is approximately $3300 \text{ J/kg}\cdot\text{K}$ (Fu et al., 2014)
- Diffusion Coefficient: The diffusion coefficient for small molecules through the dermis is typically in the range of $3.5 \times 10^{-5} \text{ cm}^2/\text{s}$, reflecting its role in facilitating nutrient and oxygen transport (Cornelissen et al., 2008).

2.3 Design 3D of the microneedle patch in SOLIDWORKS

The design and modeling process of microneedle patch was conducted using SOLIDWORKS (Figure 1). The geometry of the part was developed following the functional requirements and technical specifications of the system under study, based on parameters established in the scientific literature described in the previous sections.

The process began with the creation of a 2D sketch on a reference plane, where the primary dimensions of the needle were defined, including tip thickness, height, base width, and skin insertion depth. These dimensions were derived from previous studies (section 2.1) to ensure the design's functionality and alignment with real-world applications. From this initial sketch, revolve functions were employed to generate the 3D geometry of the needle. Subsequently, a sketch on the top of the needle was used to create the quadrangular base through the extrude function to define the needle's opening for liquid flow; shell and cut-extrude functions were applied. Finally, fillet details were added to the needle's mouth to enhance functionality and ensure smooth liquid flow by eliminating sharp edges.

The material Ti-6Al-4V (titanium alloy) was assigned to the needle, selected for its exceptional stiffness, high corrosion resistance, and biocompatibility. In parallel, three distinct pieces representing the skin layers—stratum corneum, dermis, and epidermis—were created. The material properties for these layers were defined based on data obtained from the scientific literature mentioned in section 2.2, ensuring accurate representation of each layer's mechanical and physical characteristics. These skin layers were assembled in a stacked configuration, adhering to predefined measurements for each layer. The needle was then positioned within the assembly, and the combine/delete tool was used to create the hole in the skin, representing the insertion point for the needle.

Once both the needle and skin layers were modeled, positional relationships between them were established, and corresponding reference planes were generated to ensure proper alignment. The process included an interference check and geometric constraint verification to confirm the model's compatibility with the study conditions. This step ensured that there were no overlaps or misalignments between the components. Finally, the solid model was exported in a compatible format for further analysis, maintaining dimensional precision and surface continuity throughout the process.

2.4 Mathematical problem statement for analytical and numerical solving methods

The equation used to model the transdermal drug delivery using microneedles is Fick's second law.

$$\frac{\partial C}{\partial t} = D \nabla^2 C \quad (1)$$

with the concentration function C , which depends on time and space and the diffusion coefficient D (in m^2/s).

2.4.1 Simplest model

We consider the problem in one single dimension (x-axis). The concentration function C , can be written as $C(x, t)$ and the Fick second law is simplified.

$$\frac{\partial C(x, t)}{\partial t} = D \frac{\partial^2 C(x, t)}{\partial x^2} \quad (2)$$

We also set some initial conditions to describe the problem. The initial concentration must be uniform with the concentration C_0 inside the microneedle. No flux, which means no diffusion at $x = 0$. The drug is fully absorbed at $x = L$, setting the concentration to zero :

$$C(x, 0) = C_0, \quad 0 < x < L \quad (3)$$

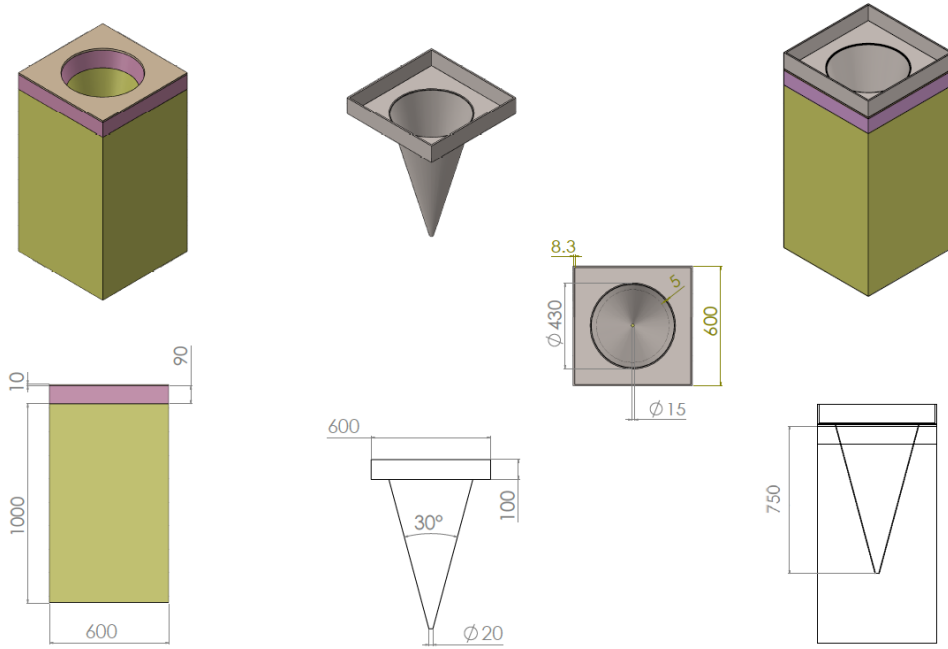


Figure 1: **Design of the microneedle patch in SOLIDWORKS.** Design in 3D of the MN patch, and the skin layers with their measures

$$\frac{\partial C(0, t)}{\partial x} = 0, \quad t > 0 \quad (4)$$

$$C(L, t) = 0, \quad t > 0 \quad (5)$$

with L the microneedle length.

2.4.2 Complex model

We extend our model by incorporating two spatial dimensions in addition to time. The environment consists of P tissue layers, each characterized by a thickness l_p and a diffusion coefficient D_p . The x -axis represents the depth in the skin and ranges from $l_0 = 0$ to $l_{tot} = \sum_{p=1}^n l_p$, while the y -axis extends from 0 to w , corresponding to the width of the studied region. The time is represented by t and goes from 0 to t_{max}

The drug is administered at $t = 0$ and is evenly distributed at a concentration C_0 in the rectangle centered on y of length L and width W .

The boundary conditions of the model are defined as follows:

- At $x = 0, y = 0$ and $y = w$, a zero-flux condition is imposed (no diffusion).
- At $x = l_{tot}$, the full absorption is assumed (zero concentration).
- At the interfaces between layers, both the concentration and the diffusive flux are continuous.

The equations governing drug diffusion in this multi-layered environment comply with these constraints and are detailed below.

$$\forall t \in \mathbb{R}^+, \quad \forall y \in [0, w], \quad \forall p \in \{1, 2, \dots, P\}, \quad \forall x \in [l_{i-1}, l_i],$$

$$\frac{\partial C(x, y, t)}{\partial t} = D_p \left(\frac{\partial^2 C(x, y, t)}{\partial x^2} + \frac{\partial^2 C(x, y, t)}{\partial y^2} \right) \quad (6)$$

recall, $l_0 = 0$

$$\forall y \in [\frac{w-W}{2}, \frac{w+W}{2}], \quad \forall x \in [0, L] \quad C(x, y, 0) = C_0 \quad (7)$$

$$\forall t \in \mathbb{R}^+, \quad \forall y \in [0, w], \quad \frac{\partial C(0, y, t)}{\partial x} = 0 \quad (8)$$

$$\forall t \in \mathbb{R}^+, \quad \forall x \in [0, l_{tot}], \quad \frac{\partial C(x, 0, t)}{\partial x} = 0 \quad (9)$$

$$\forall t \in \mathbb{R}^+, \quad \forall x \in [0, l_{tot}], \quad \frac{\partial C(x, w, t)}{\partial x} = 0 \quad (10)$$

$$\forall t \in \mathbb{R}^+, \quad \forall y \in [0, w], \quad C(l_{tot}, y, t) = 0 \quad (11)$$

$$\forall t \in \mathbb{R}^+, \quad \forall y \in [0, w], \quad \forall p = 1, 2, \dots, P-1$$

$$D_p \frac{\partial C(l_p^-, y, t)}{\partial x} = D_{p+1} \frac{\partial C(l_p^+, y, t)}{\partial x} \quad \text{and} \quad C(l_p^-, y, t) = C(l_p^+, y, t) \quad (12)$$

with l_p^- and l_p^+ respectively the left and right limit of x to l_p

2.5 COMSOL problem statement

The model was developed using COMSOL Multiphysics to simulate the diffusion of a transdermal drug delivered via a microneedle patch. The simulation incorporates the Transport of Diluted Species (tds) physics to model drug diffusion, coupled with Laminar Flow (spf) to account for fluid dynamics within the skin layers. A time-dependent study was used to analyze the drug concentration distribution over a period of 24 hours, matching the time frame used in the Python simulation.

2.5.1 Geometry and Layers

The geometry of the model consists of three layers representing the skin: the Stratum Corneum, Epidermis, and Dermis. Each layer was assigned specific material properties and parameters, as described in Section 2.2 of this report. A triangular-shaped microneedle was modeled and inserted into the skin layers. The microneedle has a length of 750 μm , a base diameter of 420 μm , and a tip diameter of 15 μm . This geometry was designed to replicate the dimensions used in similar studies, ensuring consistency with experimental and computational references.

2.5.2 Boundary Conditions

The boundary conditions were defined as follows:

- No-Flux Boundary Condition: Applied to all external boundaries of the skin layers to simulate an impermeable barrier, preventing drug loss from the sides and bottom of the domain.
- Flux Boundary Condition: Applied only at the tip of the microneedle to model drug release into the skin. The flux value was set to 0.00044 mol/m²•s (Waghule et al., 2019) based on references where authors used microneedles with similar dimensions and experimental conditions.
- Concentration Condition: Applied to all the walls of the skin and the wall of the MN as concentration=0

2.5.3 Domains and Parameters

The simulation focused on the Epidermis and Dermis layers, as these are the primary regions where drug diffusion occurs. The Stratum Corneum was included in the geometry but was not considered a domain for drug diffusion due to its low permeability. The fluid velocity within the skin layers was set to 1.5×10^{-6} m/s (Jiang & Lillehoj, 2020), a value consistent with literature references for similar transdermal drug delivery systems.

2.5.4 Simulation Time

The simulation was run for a total duration of 24 hours, matching the time frame used in the Python simulation. This allowed for a direct comparison of the drug concentration profiles and diffusion behavior between the two modeling approaches.

2.6 Focus topic

By modeling this problem, we aim to analyze the role, significance, and impact of each parameter. For instance, by varying the diffusion coefficients, layer thicknesses, and microneedle dimensions while computing the total delivered drug quantity, we can determine which parameters have the greatest influence on the system. The objective is to identify the key factors that govern transdermal drug delivery based on the results of our model.

3 Methods

3.1 Analytical method

The analytical solution will allow us to validate our numerical modelisation by comparing both on a graph. We will solve the 'Simplest model' described in section 2.4.1.

We will use the Laplace transforms to solve the model.

Recall that the Laplace transform is defined as $\mathcal{L}(f)(s) = \int_0^{+\infty} f(t)e^{-ts} dt$.
And the derivative property $\mathcal{L}(f')(s) = z\mathcal{L}(f)(s) - f(0)$

So we get from (2) and using (3):

$$\mathcal{L}\left(\frac{\partial C(x,t)}{\partial t}\right) = \mathcal{L}(D \frac{\partial^2 C(x,t)}{\partial x^2}) \quad (13)$$

$$\iff sC(x,s) - C(x,0) = sC(x,s) - C_0 = D \frac{\partial^2 C(x,s)}{\partial x^2} \quad (14)$$

The general solution is of the form :

$$C(x,s) = Ae^{x\sqrt{s/D}} + Be^{-x\sqrt{s/D}} + \frac{C_0}{s} \quad (15)$$

Applying the initial conditions (4) and (5), we get :

$$A = -\frac{C_0}{2.s.cosh(\sqrt{sD/L})}, B = -\frac{C_0}{2.s.cosh(\sqrt{sD/L})} \quad (16)$$

Finally, injecting (14) into (13), we have :

$$C(x, s) = -\frac{C_0}{2.s.cosh(\sqrt{sD/L})}(e^{x\sqrt{s/D}} + e^{-x\sqrt{s/D}}) + \frac{C_0}{s} \quad (17)$$

We can compute the inverse Laplace transform to get $C(x, t)$.

$$C(x, t) = \frac{1}{2\pi i} \cdot \int_{-\infty}^{+\infty} C(x, s) e^{st} ds = \sum_{i=1}^n Res_{s_i} C(x, s) e^{st} \quad (18)$$

We can find that the residue at pole $s = 0$ is equal to 0 and that the other poles are determined by the equation :

$$\cosh(\sqrt{\frac{s}{D}}L) = 0 \iff s = -\frac{(2n+1)^2\pi^2 D}{4L^2}, n \in \mathbb{N} \quad (19)$$

$$\iff R = \frac{2(-1)^{2+n}C_0(e^{\frac{i(2n+1)\pi x}{2L}} + e^{-\frac{i(2n+1)\pi x}{2L}})e^{-D\frac{(2n+1)^2\pi^2}{4L^2}t}}{(2n+1)\pi} \quad (20)$$

Finally, we have :

$$C(x, t) = \sum_0^{\infty} \frac{2(-1)^{2+n}C_0(e^{\frac{i(2n+1)\pi x}{2L}} + e^{-\frac{i(2n+1)\pi x}{2L}})e^{-D\frac{(2n+1)^2\pi^2}{4L^2}t}}{(2n+1)\pi} \quad (21)$$

3.2 Numerical simplest model

We will use the standard finite difference method (FDM) to numerically solve our modelisation. The implementation of the numerical method is made using Python with the numpy and matplotlib libraries.

We will first discretize the present problem, cutting the x-axis in $N+1$ values and the time in $M+1$ values. We have $x_i = (i-1)\Delta x$ and $t_j = (j-1)\Delta t$ such that $i = 1, 2, \dots, N+1$ with $x_0 = 0$ and $x_{N+1} = L$ and $j = 1, 2, \dots, M+1$ with $t_0 = 0$ and $t_{M+1} = t_{max}$.

Let us denote $C(x_i, t_j) = C_i^j$. We have, using the FDM :

$$\frac{\partial C(x_i, t_j)}{\partial t_i} = \frac{C_i^{j+1} - C_i^j}{\Delta t} \quad (22)$$

and

$$\frac{\partial^2 C(x_i, t_j)}{\partial x_i^2} = \frac{C_{i+1}^j - 2C_i^j + C_{i-1}^j}{\Delta x^2} \quad (23)$$

From these two equations, we can find a formula to compute C_i^{j+1} :

$$C_i^{j+1} = C_i^j + \frac{D\Delta t}{\Delta x^2}(C_{i+1}^j - 2C_i^j + C_{i-1}^j) \quad (24)$$

$\alpha = \frac{D\Delta t}{\Delta x^2} < 0.5$ is a necessary condition for the FDM to be stable. It is the Von Neumann stability criterion.

The initial conditions give us, to translate equations (3), (4) and (5), respectively :

$$\forall i = 1, 2, \dots, N+1, \quad C_i^0 = C_0 \quad (25)$$

$$\forall j = 1, 2, \dots, t_{max}/\Delta x, \quad C_1^j = C_0^j \quad (26)$$

$$\forall j = 1, 2, \dots, t_{max}/\Delta x, \quad C_N^j = 0 \quad (27)$$

with -1 to represent the last value.

Equations (22), (23), (24) and (25) allow us to implement the simulation in Python, you can find it on GitHub, *compute_C1_matrix* function : METTRE LE LIEN

3.3 Numerical complex model

This section describes how Section 2.4.2 is implemented in Python using again the Finite Difference Method (FDM). We first discretize the problem, the x-axis has N_x values with $i = 1, 2, \dots, N_x$ such that $x_i = (i-1)\Delta x$ and $\Delta x = \frac{l_{tot}}{N_x}$. The y-axis has N_y values $j = 1, 2, \dots, N_y$ such that $y_j = (j-1)\Delta y$ and $\Delta y = \frac{w}{N_y}$. Finally, the time axis is discretized with M values with $k = 1, 2, \dots, M$ such that $t_k = (k-1)\Delta t$ and $\Delta t = \frac{t_{max}}{M}$. We also have P layers of diffusion coefficient D_p and length l_p

From (1), we get :

$$\frac{\partial C(x, y, t)}{\partial t} = D_x \frac{\partial^2 C(x, y, t)}{\partial x^2} + D_y \frac{\partial^2 C(x, y, t)}{\partial y^2} = D \left(\frac{\partial^2 C(x, y, t)}{\partial x^2} + \frac{\partial^2 C(x, y, t)}{\partial y^2} \right) \quad (28)$$

supposing that $D_x = D_y = D$

Let us denote $C(x_i, y_j, t_k) = C_{i,j}^k$. Using FDM, we get :

$$\frac{C_{i,j}^{k+1} - C_{i,j}^k}{\Delta t} = D \left(\frac{C_{i+1,j}^k - 2C_{i,j}^k + C_{i-1,j}^k}{\Delta x^2} + \frac{C_{i,j+1}^k - 2C_{i,j}^k + C_{i,j-1}^k}{\Delta y^2} \right) \quad (29)$$

$$\iff C_{i,j}^{k+1} = C_{i,j}^k + \alpha_x (C_{i+1,j}^k - 2C_{i,j}^k + C_{i-1,j}^k) + \alpha_y (C_{i,j+1}^k - 2C_{i,j}^k + C_{i,j-1}^k) \quad (30)$$

with $\alpha_x = \frac{D\Delta t}{\Delta x^2}$, $\alpha_y = \frac{D\Delta t}{\Delta y^2}$. The necessary condition for the FDM to be stable is $\alpha_x + \alpha_y < \frac{1}{2}$. It is the Von Neumann stability criterion.

We will now translate equations (7), (8), (9), (10), (11) and (12) for our FDM.

$$\forall i = 1, \dots, \lfloor L/\Delta x \rfloor, \quad \forall j = \lfloor \frac{w-W}{2}\Delta y \rfloor, \dots, \lfloor \frac{w+W}{2}\Delta y \rfloor \quad C_{i,j}^0 = C_0 \quad (31)$$

with $\lfloor . \rfloor$, the function rounds a real number to the nearest integer.

$$\forall j = 1, \dots, N_y, \quad \forall k = 1, \dots, M, \quad \frac{C_{1,j}^k - C_{0,j}^k}{\Delta x} = 0 \iff C_{0,j}^k = C_{1,j}^k \quad (32)$$

$$\forall i = 1, \dots, N_x, \quad \forall k = 1, \dots, M, \quad C_{i,0}^k = C_{i,1}^k \quad (33)$$

$$\forall i = 1, \dots, N_x, \quad \forall k = 1, \dots, M, \quad C_{i,N_y}^k = C_{i,N_y-1}^k \quad (34)$$

$$\forall j = 1, \dots, N_y, \quad \forall k = 1, \dots, M, \quad C_{N_x,j}^k = 0 \quad (35)$$

Let us introduce $i^* = \lfloor l_p \Delta x \rfloor$

$$\forall p = 1, \dots, P, \quad \forall j = 1, \dots, N_y, \quad \forall k = 1, \dots, M,$$

$$D_p \frac{C_{i^*,j}^k - C_{i^*-1,j}^k}{\Delta x} = D_{p+1} \frac{C_{i^*+1,j}^k - C_{i^*,j}^k}{\Delta x} \iff C_{i^*,j}^k = \frac{D_p C_{i^*-1,j}^k + D_{p+1} C_{i^*+1,j}^k}{D_p + D_{p+1}} \quad (36)$$

All these equations describe the Complex model and can be used and implemented in Python. You can find the code on GitHub, look at *compute_C4_matrix_2D* function : METTRE LE LIEN

3.4 COMSOL modelisation

For the COMSOL simulation, the parameters described in Section 2.5 were maintained as constants throughout the study. These parameters include material properties, base diameter, tip diameter, tip angle, diffusion coefficients, and boundary conditions, ensuring consistency across all simulations. However, to analyze the impact of microneedle length and fluid dynamics on drug diffusion, two key variables were systematically varied:

1. Microneedle Length: The length of the microneedle was adjusted to 300 μm , 500 μm , and 900 μm to study its influence on drug delivery efficiency and concentration profiles within the skin layers. These variations allowed for a comprehensive analysis of how microneedle geometry affects the diffusion process.
1. Inlet Velocity: For the microneedle with a length of 750 μm , the inlet velocity was varied to $1.5 \times 10^{-4} \text{ m/s}$ and $1.5 \times 10^{-8} \text{ m/s}$. This range of velocities was chosen to evaluate the effect of fluid flow on drug transport and distribution within the skin. The lower velocity ($1.5 \times 10^{-8} \text{ m/s}$) represents a near-static condition, while the higher velocity ($1.5 \times 10^{-4} \text{ m/s}$) simulates a more dynamic flow scenario.

4 Results

4.1 Analytical and numerical method provide same results

We will compare our numerical program, coded with the equations from the Section 3.2 with the analytical solution found in Section 3.1. Let us introduce first the table containing the values taken.

Table 1: Parameters for the comparison

Parameters	Values
Durations, t_{max} (s)	24, 48 and 72×3600
Diffusion coefficient, D ($\text{cm}^2 \cdot \text{s}^{-1}$)	5×10^{-8}
Initial drug concentration, C_0 (mg.ml^{-1})	15.8
Microneedle length, L (cm)	0.015

The following graph was obtain with python using the library Matplotlib.pyplot.

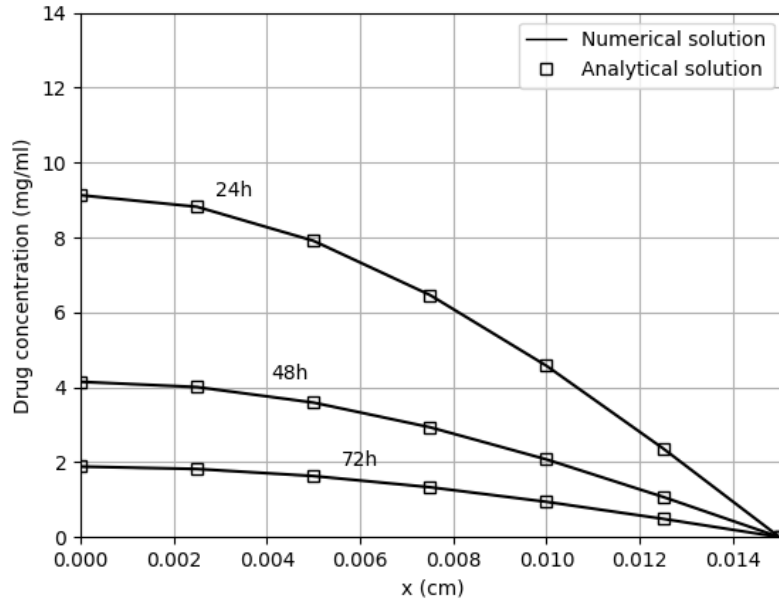


Figure 2: Comparison between numerical and analytical solution

We observe that our numerical solution aligns perfectly with the true solution obtained from the analytical model. This strong agreement allows us to confidently conclude that our numerical model is both accurate and provides a reliable description of transdermal drug delivery. With this foundation in place, we can now proceed with a detailed analysis of the results from both the Simplest and the Complex models.

4.2 Results of the Simplest model

We will now investigate the effects of all the model parameters: the diffusion coefficient, the initial concentration, and the microneedle length. Finally, we will analyze the drug delivery profiles for different diffusion coefficients.

4.2.1 Analysis of the effect of diffusion coefficient

Let us investigate the role of the diffusion coefficient in our environment. Firstly, we will introduce the table of values used for the simulation.

Table 2: Parameters for the comparison

Parameters	Values
Duration, t_{max} (s)	24 x 3600
Diffusion coefficients, D ($cm^2.s^{-1}$)	$1 \times 10^{-7}, 5 \times 10^{-8}, 1 \times 10^{-8}, 5 \times 10^{-9}$
Initial drug concentration, C_0 ($mg.ml^{-1}$)	15.8
Microneedle length, L (cm)	0.015

The results are in the figure bellow.

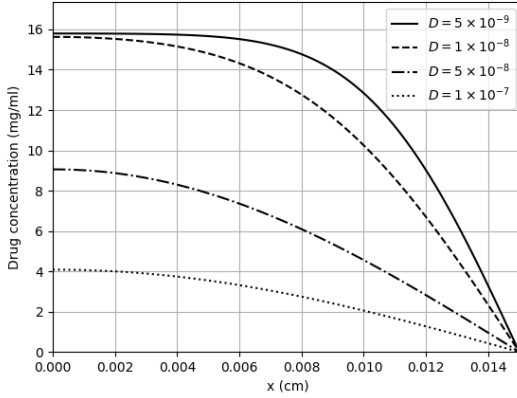


Figure 3: Distribution of drug concentration over x-axis for different diffusion coefficients

The effect of diffusion coefficient (D) in the environment is clear in this figure. Indeed, increases in diffusion coefficient (D) leads to a decrease in remaining amount of drug at a fixed position.

4.2.2 Analysis of the effect of initial concentration

Let us investigate the effect of changing initial concentration in our environment. Firstly, we will introduce the table of values used for the simulation.

Table 3: Parameters for the comparison

Parameters	Values
Duration, t_{max} (s)	24 x 3600
Diffusion coefficients, D ($cm^2.s^{-1}$)	5×10^{-8}
Initial drug concentration, C_0 ($mg.ml^{-1}$)	13.8, 14.8, 15.8, 16.8
Microneedle length, L (cm)	0.015

The results are in the figure bellow.

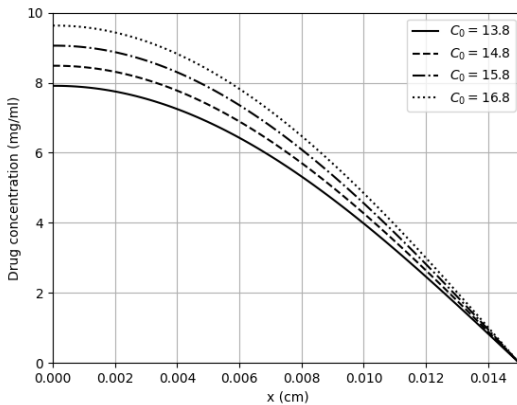


Figure 4: Distribution of drug concentration over x-axis for different initial concentrations

Increases in initial concentration (C_0) leads to an increase of remaining amount of drug for a fixed position. We can also observe that, for a fixed time t_{max} , changing the initial concentration do not play an important role, compared to the diffusion coefficient, in the final drug concentration distribution.

4.2.3 Analysis of the effect of microneedle length

Let us investigate the role of the microneedle length in our environment. Firstly, we will introduce the table of values used for the simulation.

Table 4: Parameters for the comparison

Parameters	Values
Duration, t_{max} (s)	24 x 3600
Diffusion coefficients, D ($cm^2.s^{-1}$)	5×10^{-8}
Initial drug concentration, C_0 ($mg.ml^{-1}$)	13.8, 14.8, 15.8, 16.8
Microneedle length, L (cm)	0.015

The results are in the figure bellow.

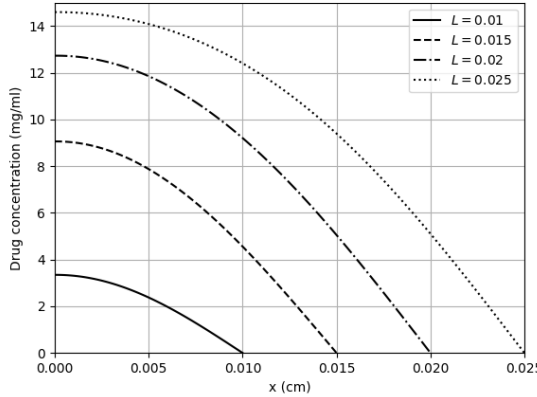


Figure 5: Distribution of drug concentration over x-axis for different initial concentrations

An increase in the microneedle length (L) results in a higher remaining drug concentration at a fixed position. However, this observation is somewhat limited. The simplest model assumes that the length of the environment (x-axis) is equal to the microneedle length, which restricts the interpretation. A more accurate analysis of the impact of microneedle length will be provided by the Complex model (see Section 4.3.3).

4.2.4 Analysis of the drug delivery profiles

Finally, for our last analysis of the Simplest model, we will study the different drug delivery profiles. Let us introduce the value table.

The results are in the figure bellow.

Table 5: Parameters for 4.2.4 analysis

Parameters	Values
Duration, t_{max} (s)	100 x 3600
Diffusion coefficients, D ($cm^2.s^{-1}$)	$1 \times 10^{-7}, 5 \times 10^{-8}, 1 \times 10^{-8}, 5 \times 10^{-9}$
Initial drug concentration, C_0 ($mg.ml^{-1}$)	15.8
Microneedle length, L (cm)	0.015

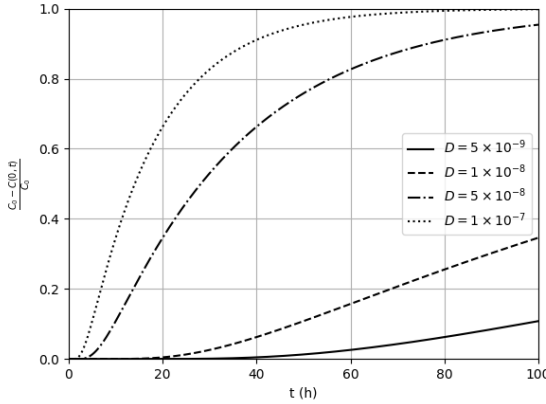


Figure 6: Drug delivery profiles

Drug delivery profiles are presented for four different diffusion coefficients. All simulated curves exhibit sustained release profiles. Notably, the diffusion coefficient has an inverse relationship with the duration of drug release: higher diffusion coefficients lead to faster drug depletion. This figure highlights the crucial role of the diffusion coefficient in drug transport. There appears to be a threshold beyond which an increase in diffusion coefficient significantly accelerates the release profile.

4.3 Results of the Complex model

In this Section, we will consider 3 layers corresponding to the stratum corneum, the epidermis and the dermis each have different parameters. Let us introduce the table of parameters that will not change for any following sub-section.

Table 6: Constant parameters of the environment

Parameters	Values
Stratum corneum length, l_1 (m)	1×10^{-5}
Epidermis length, l_2 (m)	9×10^{-5}
Dermis length, l_3 (m)	1×10^{-3}
Stratum corneum diffusion coefficient, D_1 $m^2.s^{-1}$	1×10^{-14}
Epidermis diffusion coefficient, D_2 $m^2.s^{-1}$	6.2×10^{-10}

The diffusion can be observed as a function of time with a video or 2D plots of the simulation at different time steps. Here, we will plot the diffusion with the same values as in the first table of values (Table 1), at 0, 2, 4, 6, 8 and 10 hours of diffusion.

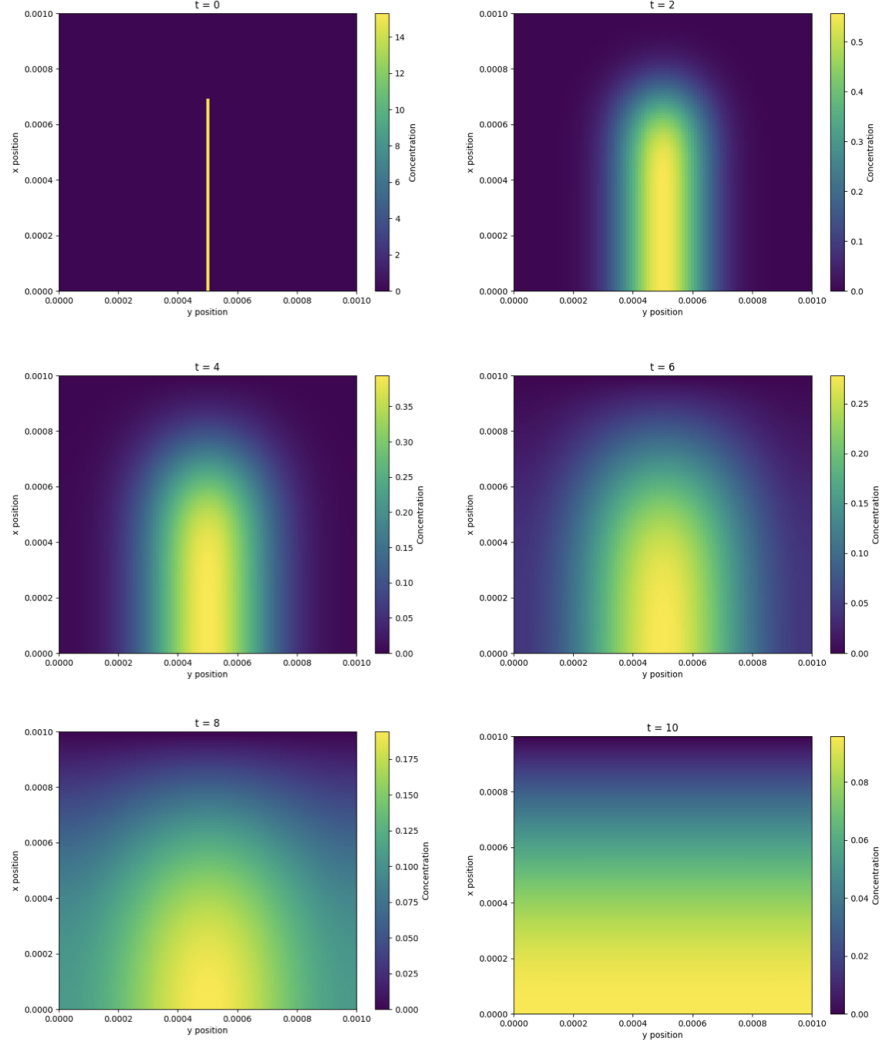


Figure 7: Distribution of drug concentration in the environment

A good metric to analyze the effect of different model parameters, that we will use for this section, is the quantity of drug delivered. This can be computed numerically by computing the discrete integral of drug concentration over space. The quantity of drug Q at time k in the environment is :

$$Q_k = \sum_{i=0}^{N_x} \sum_{j=0}^{N_y} C_{i,j}^k \quad (37)$$

Then, the quantity of drug delivered at time k is the difference between the initial quantity and the quantity at time k .

$$Q_{delivered,k} = Q_0 - Q_k \quad (38)$$

We will use this metric to analyze the same parameters as in the Simplest model, diffusion coefficient, microneedle length and initial concentration.

4.3.1 Analysis of the effect of diffusion coefficient

Let us investigate the role of the diffusion coefficient in the Complex model. The table of values is the same as the one in Section 4.2.1, simply, the diffusion coefficients values refers to the dermis diffusion coefficients D_3 .

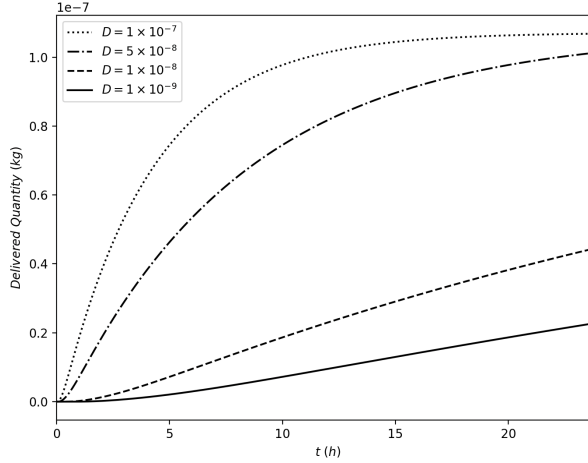


Figure 8: **Quantity of drug delivered in function of the time for different diffusion coefficients (D) values**

4.3.2 Analysis of the effect of microneedle length

Let us now study the effect of the microneedle length in the Complex model. The table of values is the same as the one in Section 4.2.3, simply, the diffusion coefficient values refers to the dermis diffusion coefficient D_3 .

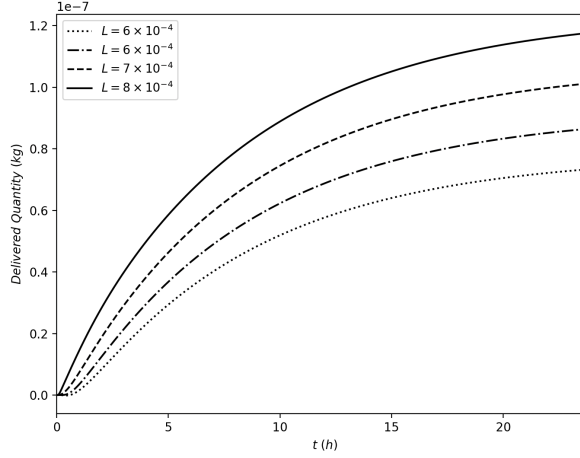


Figure 9: **Quantity of drug delivered in function of the time for different microneedle length (L) values**

4.3.3 Analysis of the effect of initial concentration

Let us observe the role of the initial concentration in the Complex model. The table of values is the same as the one in Section 4.2.2, simply, the diffusion coefficient values refers to the dermis diffusion coefficient D_3 .

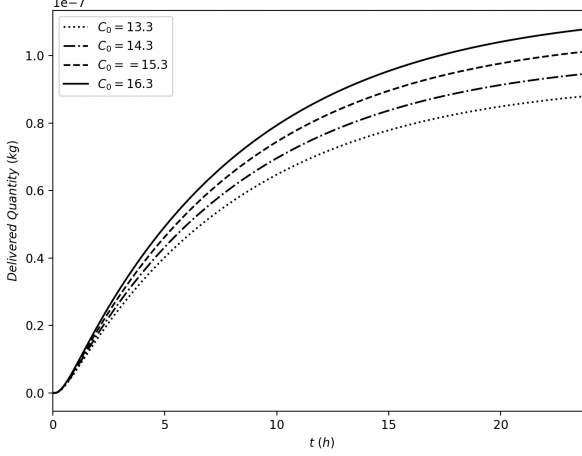


Figure 10: **Quantity of drug delivered in function of the time for different initial concentration (C0) values**

4.4 Results on COMSOL

4.4.1 Microneedle lenght

The results of the COMSOL model using different MN lengths are shown in Figure 11. The MN with a length of 300 μm (Fig. 11A & 11B) shows a relatively shallow penetration depth and a good and rapid diffusion through all the skin layers. In addition, it has a final concentration of 370 mol/m^3 , which is the smallest concentration of all the models. On the other hand, the MN of 500 μm (Fig. 11 C & 11D) shows a deeper penetration compared to the 300 μm microneedle with a final concentration slightly higher of the 300 μm MN with a value of 386 mol/m^3 and with a very good diffusion profile through the skin layer. Conversely, the 750 μm MN (Fig. 11E & 11F) achieved significantly deeper penetration compared to the 300 μm and 500 μm microneedles, and reach a notably improvement in the final concentration with a value of 412 mol/m^3 . However, the diffusion of the drug through the skin layer it's not very good and rapid compared to the previous MN lengths. Finally, the 900 μm MN (Fig. 11G & 11H) reached the highest concentration with a value of 431 mol/m^3 but has the poorest diffusion performance through the dermis because the drug is concentrated under the microneedle and it not distribute very well in all the skin.

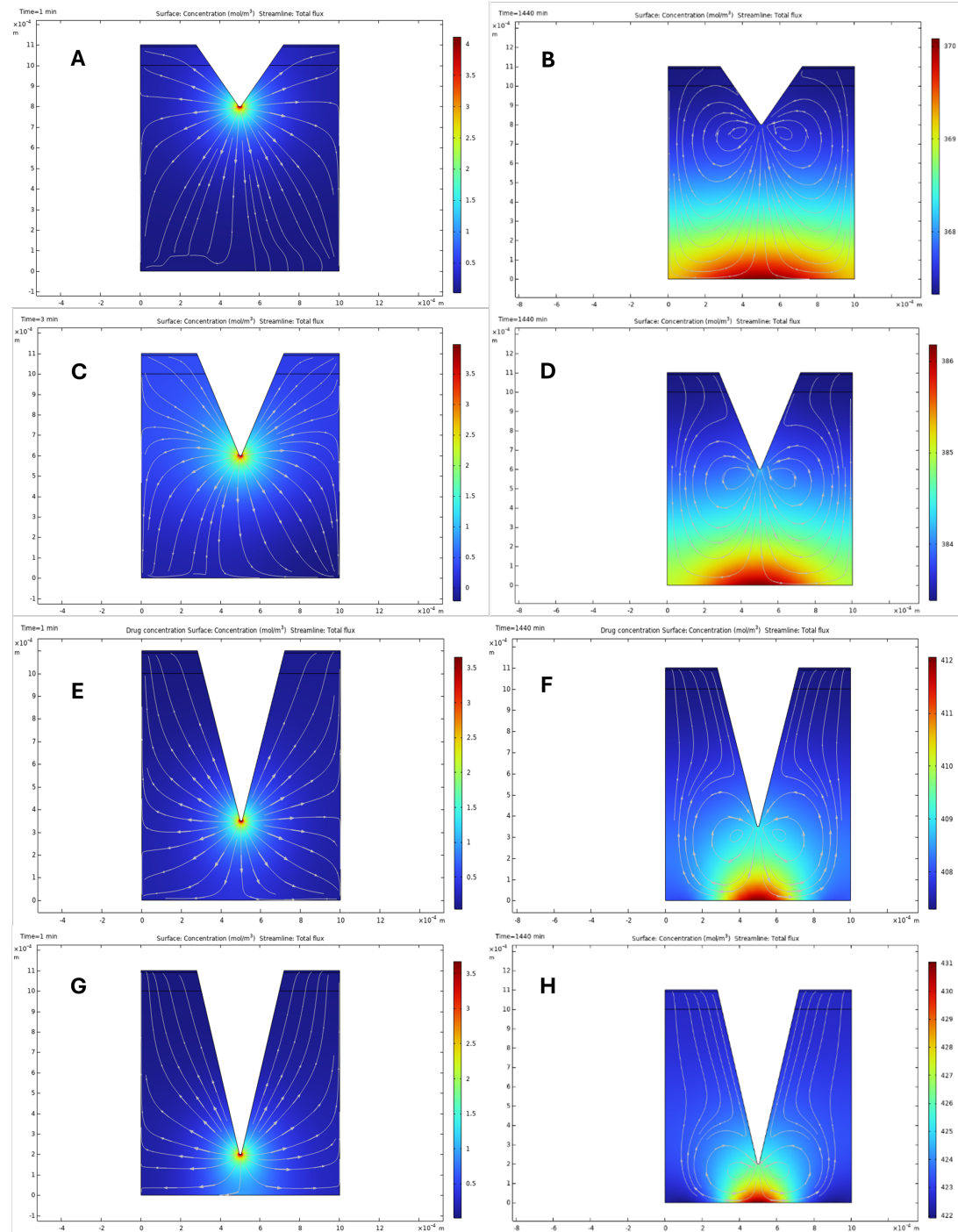


Figure 11: Drug concentration profile with different MN length (A) Concentration at $t=0$ with MN length = 300 μm . (B) Concentration at $t=24$ h with MN length = 300 μm . (C) Concentration at $t=0$ with MN length = 500 μm . (D) Concentration at $t=24$ h with MN length = 500 μm . (E) Concentration at $t=0$ with MN length = 750 μm . (F) Concentration at $t=24$ h with MN length = 750 μm . (G) Concentration at $t=0$ with MN length = 900 μm . (H) Concentration at $t=24$ h with MN length = 900 μm .

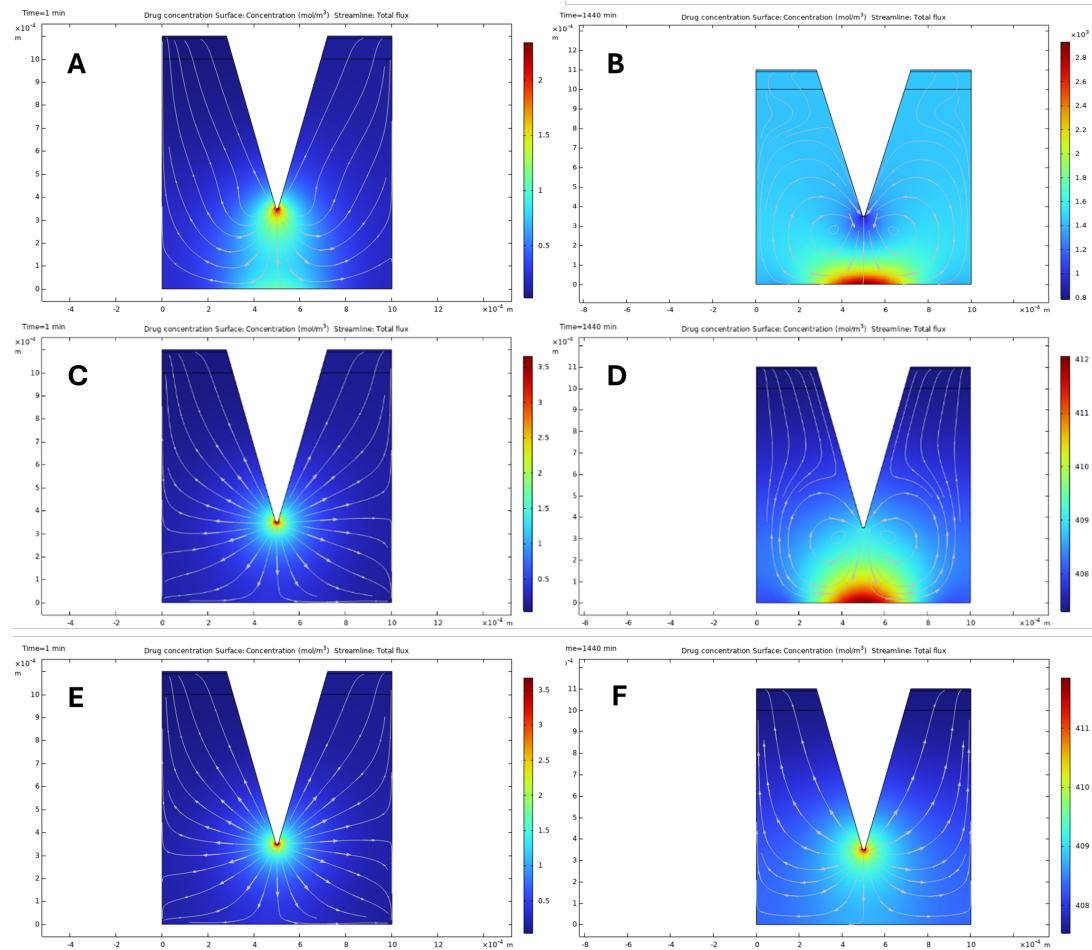


Figure 12: Drug concentration with different inlet velocity in 750 μm MN. (A) Concentration at $t=0$ with inlet velocity = 1.5×10^{-4} m/s. (B) Concentration at $t=24$ h with inlet velocity = 1.5×10^{-4} m/s. (C) Concentration at $t=0$ with inlet velocity = 1.5×10^{-6} m/s. (D) Concentration at $t=24$ h with inlet velocity = 1.5×10^{-6} m/s. (E) Concentration at $t=0$ with inlet velocity = 1.5×10^{-8} m/s. (F) Concentration at $t=24$ h with inlet velocity = 1.5×10^{-8} m/s.

4.4.2 Intlet velocity

The results of the COMSOL model using different inlet velocities in the 750 μm MN are shown in Figure 12. The drug concentration profile with inlet velocity of 1.5×10^{-4} m/s (Fig. 12A & 12B) is the highest inlet velocity, shows a concentration significantly very high since the time 0 in all the skin layers and with a final concentration of 2800 mol/m³. On the other side, the concentration of the inlet velocity 1.5×10^{-6} m/s (Fig. 12C & 12D) shows a moderate drug penetration and distribution with a concentration notably smaller than the drug concentration with inlet velocity of 1.5×10^{-4} m/s, at the end of the simulation the concentration reached a value of 412 mol/m³ at the bottom of the dermis layer. Finally, the profile with the lowest inlet velocity of 1.5×10^{-8} m/s (Fig. 12E & 12F) has a very low concentration even at time =24 h, where it can be observed that almost all the drug remained in the tip of the microneedle and hardly diffused through the skin layers.

5 Critique and summary

5.1 Critiques on the numerical model

The numerical complex model could be improved to obtain a simulation that better describes transdermal drug delivery. One attempted improvement, which did not succeed, was changing the way the drug injection is modeled. In the current model, we consider a uniform concentration (C_0) of the drug where the microneedle is positioned. A more accurate modeling approach would be to consider an injection with a flux at the tip of the microneedle. This approach was implemented but did not yield satisfactory results.

Another possible improvement would be to perform a simulation in a three-dimensional space. However, this was not implemented numerically because the 2D simulation already required a long computing time, and transitioning to a 3D simulation would have resulted in an excessively high computational cost. One way to reduce this computation time would be to use the Crank-Nicolson scheme (discussed in Section 6), but this would require rewriting the entire existing code, as it follows a different finite difference approach.

6 Recommendations for future work

To be able to implement numerically both the Simplest and Complex models, we use the finite difference method (FDM). In particular, the explicit finite difference method (EFDM) that needs a stability criterion, the Von Neumann stability criterion, for the method to be stable. Later, we found an implicit finite difference method (IFDM), the Crank-Nicolson scheme, that is more adapted to our problem. Firstly, it is better adapted to limit conditions between two layers with different diffusion coefficients. Secondly, this new method does not need a criterion to be stable because it is unconditionally stable. Also, this numerical simulation requires a lot of computing time. The EFDM has a complexity of $\mathcal{O}(NxNyM)$ but it should also satisfy the Von Neumann criterion, while the IFDM has a complexity of $\mathcal{O}(NxNyM^2)$ but does not have a criterion. But in practice, we are forced to increase the value of M (in EFDM) to a great extent for the simulation to be stable. We think that if we used the IFDM, despite the higher complexity, the final number of calculation would have been less because M is forced to be increased to satisfy the stability criterion.

Let us find the condition for the FFDM complexity to be lower than the EFDM complexity.

For a fixed number of subdivisions of the x-axis Nx and y-axis Ny, EFDM complexity is $\mathcal{O}(NxNyM^*)$ with M^* the number of subdivisions of the time satisfying the Von Neumann criterion and the IFDM complexity is $\mathcal{O}(NxNyM^2)$.

Then, the condition for the IFDM complexity to be lower than the EFDM complexity is $M^2 < M^*$.

Let us find the expression of M^* . From the Von Neumann criterion, we have :

$$\alpha_x + \alpha_y < \frac{1}{2} \quad (39)$$

But also,

$$\alpha_x + \alpha_y = \frac{D\Delta t}{\Delta x^2} + \frac{D\Delta t}{\Delta y^2} = D\Delta t \left(\frac{1}{\Delta x^2} + \frac{1}{\Delta y^2} \right) = \frac{Dt_{max}}{M^*} \left(\frac{Nx^2}{l_{tot}^2} + \frac{Ny^2}{w^2} \right) \quad (40)$$

$$\iff M^* > 2Dt_{max} \left(\frac{Nx^2}{l_{tot}^2} + \frac{Ny^2}{w^2} \right) \quad (41)$$

Considering that we take the smallest value of M^* that satisfies this equation, we recover the condition for the M of the IFDM method :

$$M^2 > 2Dt_{max}\left(\frac{Nx^2}{l_{tot}^2} + \frac{Ny^2}{w^2}\right) \iff M < \sqrt{2Dt_{max}\left(\frac{Nx^2}{l_{tot}^2} + \frac{Ny^2}{w^2}\right)} \quad (42)$$

Then, the IFDM complexity is lower than the EFDM complexity if the condition (40) is satisfied.

Now, let us take an example of numerical application to see what it represent for our case of transdermal drug delivery by taking coefficients used in our simulation. We will take $D = 10^{-8} m^2.s^{-1}$, $t_{max} = 10^5 s$ (approximately a day), $Nx = Ny = 10^2$, $l_{tot} = w = 10^{-3} m$. We compute $M^* = \sqrt{2Dt_{max}\left(\frac{Nx^2}{l_{tot}^2} + \frac{Ny^2}{w^2}\right)} = 6325$.

We can easily reduce M in an IFDM to a value like 100, which is an acceptable number for plotting a diffusion video, resulting in a significant decrease in the number of calculations.

(43)

Besides, in our modelization methods we can analyze the impact of more microneedles and rebuild our design to analyze the impact that will have more MN in the drug release and optimize our MN length to ensure a better distribution of the drug with a good final concentration profile.

7 References

1. Abdullah, A. C., Ahmadinejad, E., & Tasoglu, S. (2024). Optimizing Solid Microneedle Design: A Comprehensive ML-Augmented DOE Approach. *ACS Measurement Science Au*, 4(5),
2. Anderson, R. L., & Cassidy, J. M. (1973). Variations in physical dimensions and chemical composition of human stratum corneum. *Journal of Investigative Dermatology*, 61(1), 30-32.
3. Bao, L.; Park, J.; Bonfante, G.; Kim, B. Recent advances in porous microneedles: Materials, fabrication, and transdermal applications. *Drug Deliv. Transl. Res.* 2022, 12, 395–414
4. Barry, B. W. (2001). Novel mechanisms and devices to enable successful transdermal drug delivery. *European Journal of Pharmaceutical Sciences*, 14(2), 101-114.
5. Becker, S. (2012). Transport modeling of skin electroporation and the thermal behavior of the stratum corneum. *International Journal of Thermal Sciences*, 54, 48-61.
6. Brunette, D. M., Tengvall, P., Textor, M., & Thomsen, P. (2001). Titanium in medicine: Material science, surface science, engineering, biological responses, and medical applications. Springer.
7. Cornelissen, L. H., Bronneberg, D., Oomens, C. W., & Baaijens, F. P. (2008). Diffusion measurements in epidermal tissues with fluorescent recovery after photobleaching. *Skin research and Technology*, 14(4), 462-467.
8. Davis, S.P.; Landis, B.J.; Adams, Z.H.; Allen, M.G.; Prausnitz, M.R. Insertion of microneedles into skin: Measurement and prediction of insertion force and needle fracture force. *J. Biomech.* 2004, 37, 1155–1163.
9. Donnelly, R. F., Singh, T. R. R., Garland, M. J., Migalska, K., Majithiya, R., & McCarthy, H. O. (2012). Hydrogel-forming microneedle arrays for enhanced transdermal drug delivery. *Advanced Functional Materials*, 22(23), 4879-4890.

10. Elias, C. N., Lima, J. H. C., Valiev, R., & Meyers, M. A. (2008). Biomedical applications of titanium and its alloys. *JOM*, 60(3), 46–49.
11. Elias, P. M. (1983). Epidermal lipids, barrier function, and desquamation. *Journal of Investigative Dermatology*, 80(1), 44s–49s.
12. Ferziger, J. H., Perić, M., & Street, R. L. (2019). Computational methods for fluid dynamics. Springer.
13. Fu, M., Weng, W., & Yuan, H. (2014). Numerical simulation of the effects of blood perfusion, water diffusion, and vaporization on the skin temperature and burn injuries. *Numerical Heat Transfer, Part A: Applications*, 65(12), 1187-1203.
14. Geetha, M., Singh, A. K., Asokamani, R., & Gogia, A. K. (2009). Ti based biomaterials, the ultimate choice for orthopaedic implants – A review. *Progress in Materials Science*, 54(3), 397–425.
15. Guy, R. H., & Hadgraft, J. (2003). Transdermal Drug Delivery. Marcel Dekker. Kim, Y. C., Park, J. H., & Prausnitz, M. R. (2012). Microneedles for drug and vaccine delivery. *Advanced Drug Delivery Reviews*, 64(14), 1547-1568.
16. Jiang, X., & Lillehoj, P. B. (2020). Microneedle-based skin patch for blood-free rapid diagnostic testing. *Microsystems & nanoengineering*, 6(1), 96.
17. Kochhar, J.S.; Quek, T.C.; Soon, W.J.; Choi, J.; Zou, S.; Kang, L. Effect of Microneedle Geometry and Supporting Substrate on Microneedle Array Penetration into Skin. *J. Pharm. Sci.* 2013, 102, 4100–4108
18. Kwon, H. J., Lee, S. G., Lee, J. W., Kim, H. S., & Park, E. S. (2017). Finite element analysis of transdermal drug delivery systems. *Journal of Drug Delivery Science and Technology*, 42, 184-192.
19. Langer, R., & Peppas, N. A. (1983). Chemical and physical structure of polymers as carriers for controlled release of bioactive agents: A review. *Journal of Macromolecular Science, Part C: Polymer Reviews*, 23(1), 61-126.3
20. Leyens, C., & Peters, M. (2003). Titanium and titanium alloys: Fundamentals and applications. Wiley-VCH.
21. Li, C., Guan, G., Reif, R., Huang, Z., & Wang, R. K. (2012). Determining elastic properties of skin by measuring surface waves from an impulse mechanical stimulus using phase-sensitive optical coherence tomography. *Journal of The Royal Society Interface*, 9(70), 831-841.
22. Marquez-Lago, T. T., Allen, D. M., & Thewalt, J. (2010). A novel approach to modelling water transport and drug diffusion through the stratum corneum. *Theoretical Biology and Medical Modelling*, 7, 1-25.
23. Menon, G. K. (2002). New insights into skin structure: Scratching the surface. *Advanced Drug Delivery Reviews*, 54(1), S3–S17
24. Nagayama, K., & Kurihara, T. (2018). Numerical simulation of skin formation: the relationship between transepidermal water loss and corneum thickness. *Journal of Applied Mathematics and Physics*, 6(8), 1757-1762
25. Niinomi, M. (2008). Mechanical biocompatibilities of titanium alloys for biomedical applications. *Journal of the Mechanical Behavior of Biomedical Materials*, 1(1), 30–42.
26. Oliveira, C., Teixeira, J. A., Oliveira, N., Ferreira, S., & Botelho, C. M. (2024). Microneedles' device: design, fabrication, and applications. *Macromol*, 4(2), 320-355.

27. Park, J.-H.; Prausnitz, M. Analysis of mechanical failure of polymer microneedles by axial force. *J. Korean Phys. Soc.* 2010, 56, 1223–1227.
28. Pletcher, R. H., Tannehill, J. C., & Anderson, D. (2012). Computational fluid mechanics and heat transfer. CRC press.
29. Prausnitz, M. R., & Langer, R. (2008). Transdermal drug delivery. *Nature Biotechnology*, 26(11), 1261-1268.
30. Prausnitz, M. R., Mitragotri, S., & Langer, R. (2004). Current status and future potential of transdermal drug delivery. *Nature Reviews Drug Discovery*, 3(2), 115-124.
31. Proksch, E., Brandner, J. M., & Jensen, J. M. (2008). The skin: An indispensable barrier. *Experimental Dermatology*, 17(12), 1063–1072
32. Romgens, A.; Bader, D.; Bouwstra, J.; Baaijens, F.; Oomens, C. Monitoring the penetration process of single microneedles with varying tip diameters. *J. Mech. Behav. Biomed. Mater.* 2014, 40, 397–405.
33. Sabri, A.H.; Kim, Y.; Marlow, M.; Scurr, D.J.; Segal, J.; Banga, A.K.; Kagan, L.; Lee, J.B. Intradermal and transdermal drug delivery using microneedles—Fabrication, performance evaluation and application to lymphatic delivery. *Adv. Drug Deliv. Rev.* 2020, 153, 195–215.
34. Scheuplein, R. J., & Blank, I. H. (1971). Permeability of the skin. *Physiological Reviews*, 51(4), 702-747.
35. Sorrell, J. M., & Caplan, A. I. (2004). Fibroblast heterogeneity: More than skin deep. *Journal of Cell Science*, 117(5), 667–675.
36. Thomas, J. W. (2013). Numerical partial differential equations: finite difference methods (Vol. 22). Springer Science & Business Media.
37. Verbaan, F.J.; Bal, S.M.; Van den Berg, D.J.; Groenink, W.H.H.; Verpoorten, H.; Luttge, R.; Bouwstra, J.A. Assembled microneedle arrays enhance the transport of compounds varying over a large range of molecular weight across human dermatomed skin. *J. Control. Release* 2007, 117, 238–245.
38. Waghule, T., Singhvi, G., Dubey, S. K., Pandey, M. M., Gupta, G., Singh, M., & Dua, K. (2019). Microneedles: A smart approach and increasing potential for transdermal drug delivery system. *Biomedicine & pharmacotherapy*, 109, 1249-1258.